Journal of Marine Research, 67, 619–635, 2009

Asymmetries in tidal flow over a Seto Inland Sea scour pit

by Arnoldo Valle-Levinson[1] and Xinyu Guo[2]

ABSTRACT

Underway profiles of current velocity were combined with stationary profiles of temperature and salinity around a vertically mixed scour pit of the Seto Inland Sea throughout a semidiurnal tidal cycle. This was done with the purpose of determining (a) whether flood flow is asymmetric relative to ebb over a pit with weakly stratified conditions, and (b) whether there is a dynamic transition from frictionally dominated tidal flow to advectively dominated tidal flow over the pit. These questions arose from previous studies elsewhere under stratified water columns, in contrast to the unstratified conditions at the study site. Observations showed an acceleration of the flood tidal flow over the pit and a deceleration during ebb. The flow acceleration over the pit during flood and deceleration during ebb was attributed to asymmetric patterns of flow convergence/divergence. In turn, these divergence patterns were influenced by the direction and strength of the baroclinic pressure gradient force, which was 10 to 30% of the advective term, despite the relatively weak horizontal gradients of order 10^{-5} kg/m^4. The non-negligible influence of the baroclinic pressure gradient was possible from the relatively large depths that exceeded 100 m at the deepest part of the pit, compared to the surrounding depths of 30 m. From depth-averaged dynamical terms derived for flood and ebb phases of the tidal cycle, it was found that the advective terms became more important than frictional terms over the deep parts of the pit. Advection became more prominent than friction where the bottom slope exceeded the value of the bottom drag coefficient ($\sim$0.003). Otherwise, frictional effects dominated outside the pit.

1. Introduction

Scour pits or bathymetric hollows are depressions in the ocean floor or elongated holes that tend to be ubiquitous in estuarine systems (e.g., Davies and Brown, 2007). The location of scour pits is often related to erosive processes caused by flow accelerations around capes or headlands. Scour pits tend to be molded by the interaction of oscillatory tidal flows with coastal morphology and sometimes under the influence of water column density stratification. Oscillatory homogeneous flows moving over scour pits are expected to decelerate upon their passage over the cross-section expansion represented by increasing depths. This is analogous to flows moving past a sill (e.g., Armi, 1986). The residual flows resulting from these oscillatory flows tend to depict re-circulating cells over the pit (Park

1. Civil and Coastal Engineering Department, University of Florida, Gainesville, Florida, 32611, U.S.A. ***email: arnoldo@ufl.edu***

2. Center for Marine Environmental Studies, Ehime University, Matsuyama, Japan.

and Wang, 1991). Under stratified water columns, the flow reaction to the pit might be different than that under unstratified conditions.

An oscillatory stratified flow interacting with a scour pit produces asymmetric distributions in hydrography (salinity and temperature) and flow (e.g., Davies and Brown, 2007; Salas-Monreal and Valle-Levinson, 2009). This is also similar to a stratified flow interacting with a sill or at a contraction (e.g., Farmer and Armi, 1986; Stenstrom, 2003). The asymmetric distributions may consist of flow accelerating over the pit during flood and decelerating over it during ebb (Salas-Monreal and Valle-Levinson, 2009). Alternatively, the flow may decelerate during both phases of the tide (Davies and Brown, 2007) as it moves over the pit. The deceleration still is asymmetric, showing more deceleration during ebb phases than during flood phases. The reason for the flow acceleration over the pit during flood was hypothesized to be a convergence of mass toward the scour pit (Salas-Monreal and Valle-Levinson, 2009). However, this mechanism of mass convergence does not explain the flow asymmetry between flood and ebb tides because there is also mass convergence toward the pit during ebb.

The reason for the asymmetry was explained, on the basis of a conceptual model and numerical solutions, as being caused by the presence of a horizontal density gradient (Cheng and Valle-Levinson, 2009). The conceptual model explained that a horizontal density gradient, with a sign typical of that observed in estuaries (density decreasing landward), weakens ebb flows and enhances flood flows over the scour pit. An important aspect of the dynamics suggested by the observations in the Chesapeake Bay (Salas-Monreal and Valle-Levinson, 2009) and by the idealized numerical solutions (Cheng and Valle-Levinson, 2009), is that the flow dynamics are frictionally dominated outside the pit and transition to advectively dominated inside the pit. A scaling analysis of the dynamical terms involved in balancing the pressure gradient, i.e. advection and friction, indicates that the transition between dynamical regimes occurs over the area where the bathymetric slope equals the bottom drag coefficient ($\sim$0.003).

This work investigates, with observations, two main issues that extend the findings of the research described above. First, it determines whether the flood/ebb asymmetries caused by a horizontal density gradient over a scour pit are also observable in a system where the water column is nearly vertically homogeneous but with weak horizontal density gradients. Second, this work explores whether the transition in the dynamics from frictionally dominated flow outside the pit to advectively dominated flow over the pit is detected in a weakly stratified system. A semidiurnal tidal cycle experiment, under calm winds, was carried out over a scour pit in the highly energetic region of the Seto Inland Sea, in Japan. Horizontal density gradients in this region were of order 10^{-5} kg/m^4 or smaller. Because of the weak density gradients observed during the period of measurements, nearly symmetric distributions during ebb and flood, which are expected from homogeneous water columns, were anticipated to appear over the scour pit sampled. However, notable ebb/flood asymmetries, caused by the baroclinic pressure gradient, were observed in the

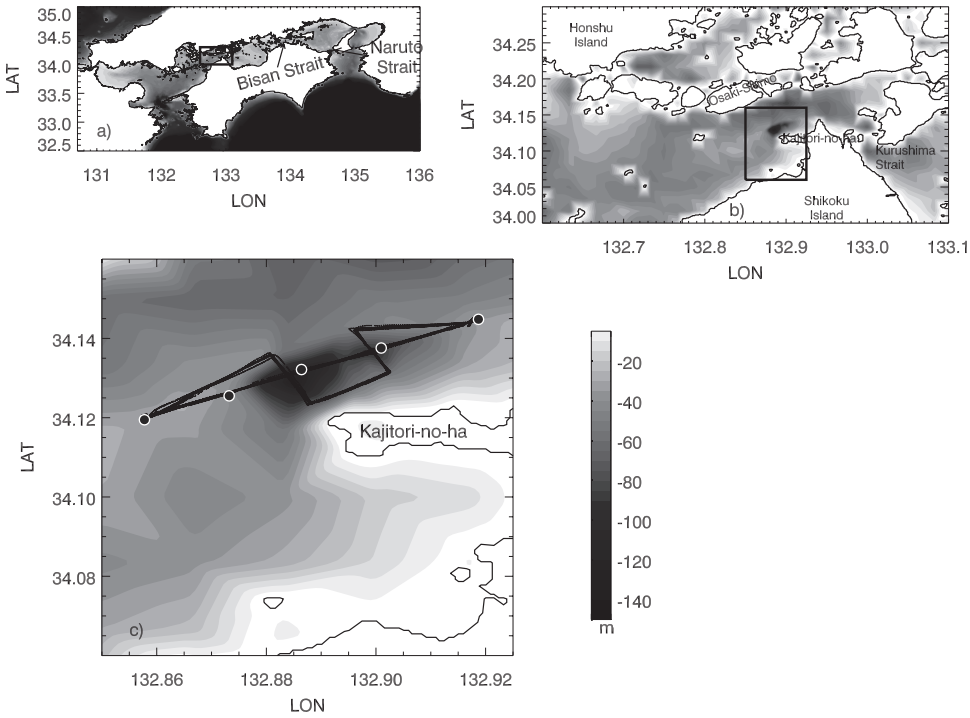

Figure 1. (a) Seto Inland Sea with bathymetry and showing area of study. (b) Zoom of the study area showing the location of the scour pit. (c) Further zoom showing sampling trajectory and location of hydrographic profiles (CTD casts marked as black circles) over the bathymetry off Kajitori no-ha.

flow. In addition, a transition was identified from frictionally dominated dynamics outside the pit to advectively dominated dynamics over the pit.

2. Study area

This study was carried out at a scour pit on Kurushima Strait, located off the northern end of Japan's Shikoku Island in the Seto Inland Sea (Fig. 1). The strait is oriented roughly in the NE-SW direction and is delimited to the NW by Osaki-Shimo Island and to the SE by Kajitori-no-Ha peninsula. Offshore of the peninsula, ~750 m to the NNW, a well-defined scour pit with a length of 5 km (along-pit direction), width of 1.5 km (cross-pit direction), and maximum depth of 120 km (Fig. 1), cuts through the surrounding depths of ~30 m. At the southwestern flank of the scour pit the depth increases from 30 m to 120 m over a distance of ~1.5 km, representing a slope of 0.06. Over the northeastern flank of the pit the bottom slope is gentler, with typical values of 0.03. The rim of the scour pit is characterized by the presence of megaripples with wavelengths of ~200 m and heights of ~6–8 m. As will be described here, those megaripples affect tidal flows.

Tides in the entire Seto Inland Sea are mixed with semidiurnal dominance. Tidal

amplitudes can reach 2 m at Kurushima Strait and Bisan Strait (Yanagi *et al.,* 1982), which are the narrowest sections in the middle part of the Inland Sea. Bisan Strait, as aside information, is at the other northward protrusion of Shikoku Island, to the east of Kurushima Strait. Tidal currents at the narrowest part of Kurushima Strait, a few hectometers farther into the Inland Sea from the scour pit, can reach more than 2 m/s while over the scour pit they can exceed 1 m/s. For reference, tidal currents can reach up to 5 m/s at Naruto Strait (Yanagi and Okaichi, 2007). The density gradients tend to be weak over the entire Seto Inland Sea because of the elevated tidal dissipation at most of the straits, where the currents accelerate and maintain a well-mixed water column. Despite the weak vertical and horizontal gradients, as will be shown here, the horizontal baroclinic pressure gradients may be influential in the dynamics of the system because its depth typically exceeds 30 m.

The geometry of the scour pit, its relatively short length and width, plus its remarkable bottom slopes, made it an ideal natural setting to sample the three-dimensional influence of a scour pit on flow distributions. Furthermore, the strength of the tidal flows (~1 m/s) in this area ensured the detection of flow alterations caused by the pit as shown next.

3. Data collection

Underway profiles of current velocity were combined with conductivity-temperature-depth (CTD) profiles at fixed stations over a scour pit in the Kurushima Strait (Fig. 1) with the purpose of describing the influence of the scour pit on tidal flows. Underway data were collected over a sampling track that cut the scour hole once in the longitudinal direction and twice in the transverse direction (Fig. 1) during one semidiurnal tidal cycle on May 31, 2007. Current velocities were collected with a 307.7 kHz RD Instruments acoustic Doppler current profiler (ADCP) mounted on a pipe attached to the starboard side of the R/V *Tobiuo* (*Flying Fish*) of Ehime University. Acoustic pings with bin depths of 2 m were recorded every second and averaged every 10 seconds while cruising at ~2 m/s. This sampling scheme yielded a spatial resolution of ~20 m in the horizontal. The first ADCP bin was centered at a depth of 2.76 m, resulting from a blanking interval of 0.6 m. The last usable bin was located at 90% of each profile depth because of side lobe effects from the angled ADCP transducers. A total of 9 transect repetitions of the along-pit transect and 7 repetitions of the two cross-pit transects were carried out during the semidiurnal sampling period.

Hydrographic profiles were obtained at 5 stations on the along-pit transect. Two stations were located at each end of the transect, outside the scour pit. One CTD station was occupied over the deepest part and two more stations were located over the slopes of the scour pit. The profiles were recorded with an Alec Instruments CTD, (ACL208-PDK) with a vertical resolution of 0.1 m and an accuracy of 0.3% for depth, ±0.02°C for temperature, and ±0.02 mS/cm for conductivity. The sampling scheme allowed a vertical resolution of 0.1 m in the CTD profiles. The 5 stations were occupied only during the first transect repetition. After identifying vertically mixed conditions at every one of the 5 stations (<0.02 top-to-bottom difference in salinity and temperature), only the stations at the end of

the transect were sampled subsequently. The salinity, temperature and density difference between these two CTD stations at the end of the transect remained relatively constant (<0.04 kg/m^3 between end stations) throughout the sampling period.

In addition to identifying instantaneous velocity fields as recorded underway, the ADCP data were time-averaged for flood periods and for ebb periods. This allowed the description of the typical distributions of flood and ebb flows over the scour pit. These average flood and ebb fields were also used to calculate depth-averaged advective accelerations and bottom frictional effects to investigate whether they changed along the transect. The CTD data were used to calculate the influence of the baroclinic pressure gradient to the depth-averaged dynamics, comparatively to the advective acceleration.

4. Data description

Sampling on both phases of the tide depicted acceleration of the tidal currents over the pit during flood and deceleration during ebb. This was attributed to asymmetric but consistent divergence patterns between flood and ebb. Such asymmetry in divergence patterns was ultimately related to the influence of the horizontal density gradient as depicted next.

a. Flood phase

Sampling over the scour pit began during the flood phase of the tidal cycle (Fig. 2a). It is clear from the along-pit section that the instantaneous flow accelerated over the pit during flood. Outside the pit, on the upstream side relative to the tidal flow, the tidal current was <0.4 m/s whereas in the deepest part of the pit, only two kilometers away, it was ~ 1 m/s. The acceleration (gradient in shades) was evident at both the surface and bottom, but was greater at the bottom and mid depths, allowing the flow to reach faster velocities (>1.2 m/s) than at the surface. As explained later, this acceleration was favored by the baroclinic pressure gradient. The cross-pit transect on the upstream side of the pit, i.e. to the southwest of the deepest point of the pit, showed lateral convergence and a spiraling effect in the vertical plane (Fig. 2b). The lateral flow from the headland located to the south of the pit added mass to the hollow. The figure shows how the lateral flow cascaded down to the deepest part of the pit while decelerating from ~ 0.5 m/s to ~ 0.1 m/s. The lateral cascading developed on both flanks of the pit and favored the spiraling recirculation mentioned above. Analogously, the cross-pit transect on the downstream side of the pit, i.e., to the northeast of deepest point of the pit, displayed lateral divergence (Fig. 2c). This was related to the flood flow expanding laterally to the sides of the pit as it moved past the deepest point.

Consistent with the quasi-instantaneous snapshots captured during sampling, the average flood flows showed along-pit flow acceleration over the pit (Fig. 3a) synchronized with lateral flow convergence on the upstream side (Fig. 3b) and divergence on the downstream side of the pit (Fig. 3c). The longitudinal transect showed greatest flood flows in the scour

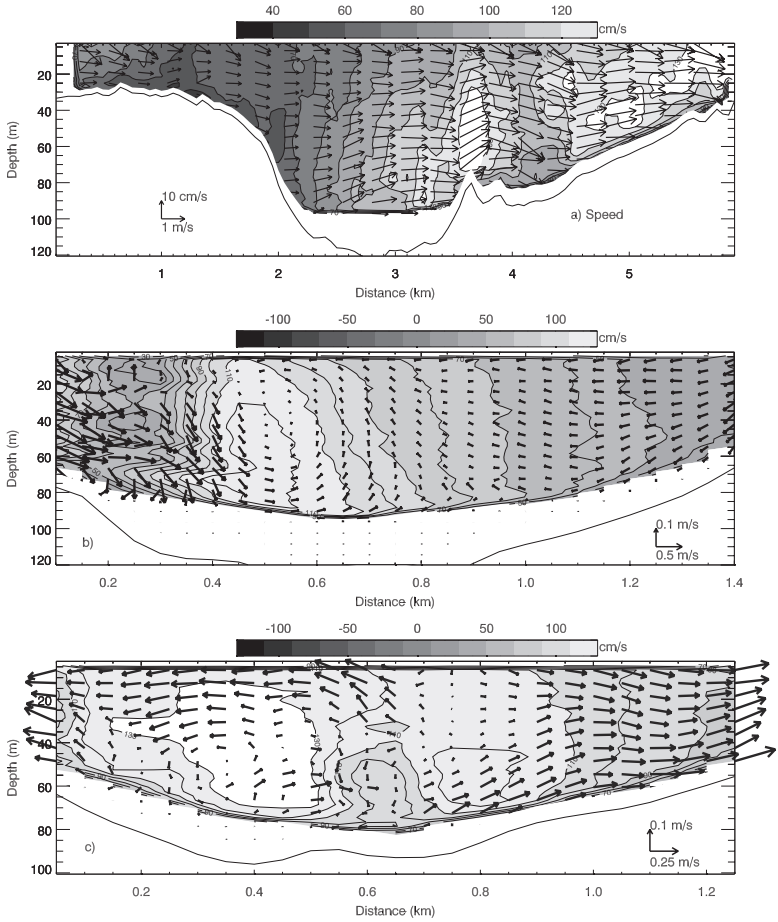

Figure 2. Instantaneous flow during flood phase of the tidal cycle. (a) Along-pit section (SW is to the left) showing flow acceleration in the deepest part of the pit. The along-pit flow is shown in shades and in arrows, moving from left to right during flood. (b) Cross-pit section on the southwestern (upstream relative to the flood flow) side of the pit showing flow convergence (looking toward the SW). Arrows represent lateral flow and shaded contours represent along-pit flow moving toward the observer. (c) Cross-pit section on the northeastern side of the pit showing flow divergence (looking toward the SW). Arrows represent lateral flow and shaded contours represent along-pit flow moving toward the observer.

pit, but concentrating near the bottom (Fig. 3a). This transect also displayed increased speeds as the flood flow moved to shallower depths over the downstream end of the pit. The lateral transects showed that on the upstream side of the pit, the greatest flood flow appeared on the deepest part of the cross-section (Fig. 3b) but was displaced to the side slopes on the downstream cross-section (Fig. 3c). The scenario of convergence of flow

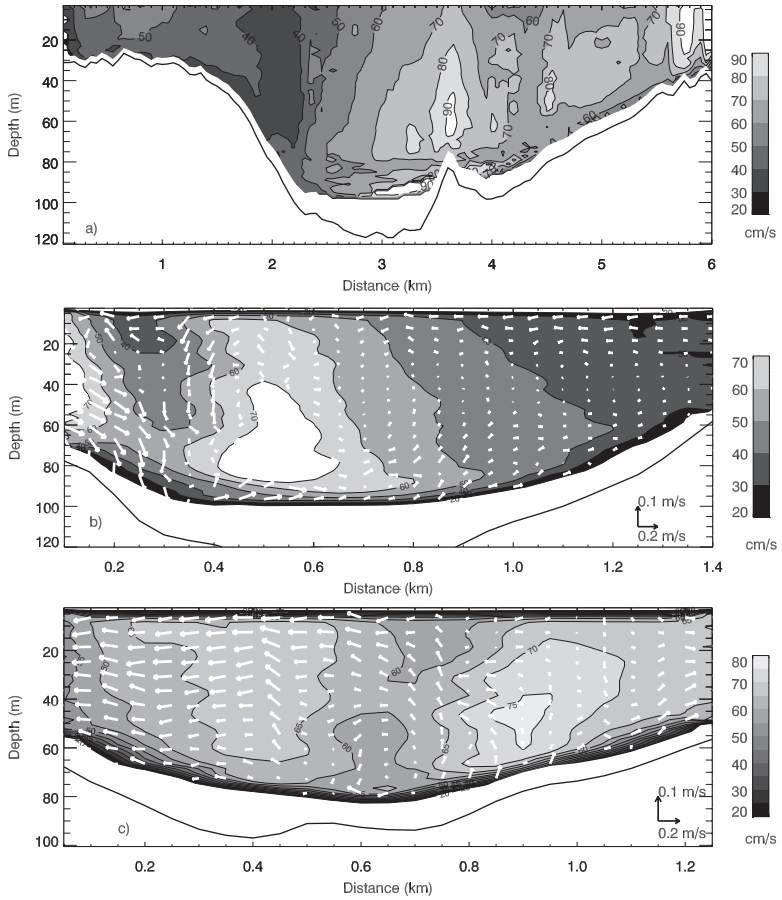

Figure 3. Same as Figure 2 but showing averages for the entire flood phase of the tidal cycle. Flow moves from left to right on (a) and toward the observer on (b) and (c).

upstream of the pit and downstream divergence was also apparent during the ebb phase but it was less robust than in flood. This is depicted next.

b. Ebb phase

The instantaneous flow pattern during the ebb phase of the tidal cycle was asymmetric with respect to that during flood. During ebb, the instantaneous flow speed decreased from around 1 m/s outside the pit to <0.5 m/s in the deepest part (Fig. 4a). Ebb flows then accelerated again as they moved on to shallow water. Upstream of the deepest part of the pit relative to ebb flow, to the northeast of the pit, the cross-pit section showed flow convergence patterns (Fig. 4c). The lateral flows during ebb were weaker than during flood and the recirculation on the vertical plane was not as well defined as that observed in flood (Fig. 2b). Nonetheless, this pattern indicated addition of mass to the pit just upstream of the

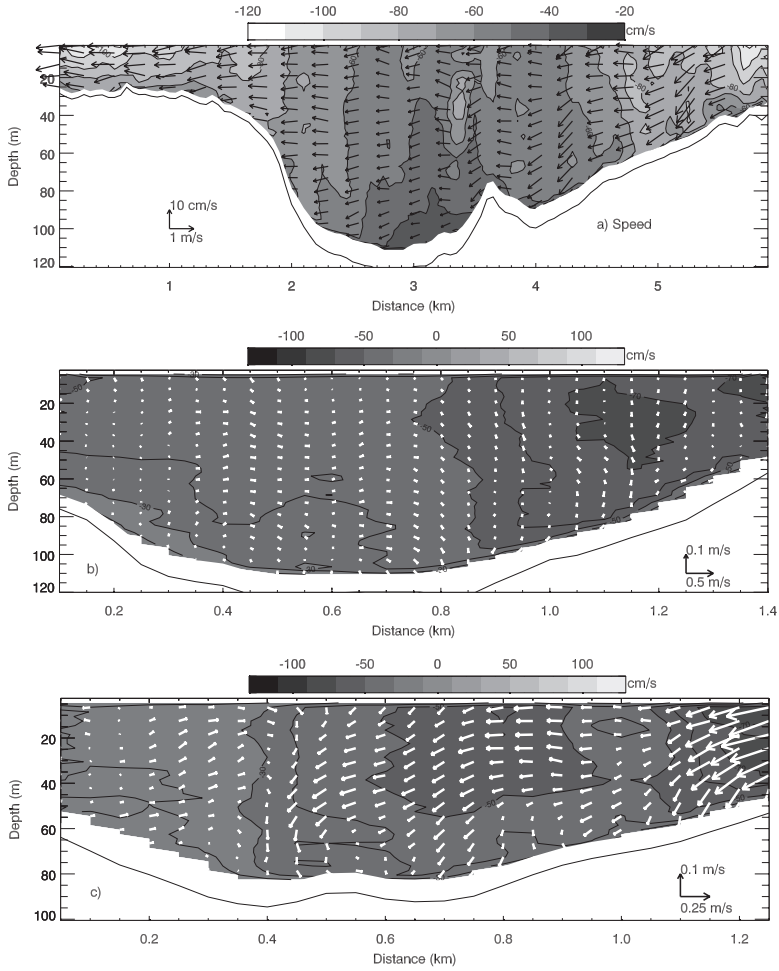

Figure 4. Instantaneous flow during ebb phase of the tidal cycle. (a) Along-pit section (SW is to the left) showing flow deceleration in the deepest part of the pit. The along-pit flow is shown in shaded contours and in arrows, moving from right to left during ebb. (b) Cross-pit section on the southwestern side of the pit showing flow divergence (looking toward the SW). (c) Cross-pit section on the northeastern (upstream relative to the ebb flow) side of the pit showing flow convergence (looking toward the SW). Arrows in (b) and (c) represent lateral flow and shaded contours represent along-pit flow moving away from the observer.

deepest part. Downstream of the deepest part of the pit, relative to the ebb flow, the cross-pit section showed weak lateral flows with a vague pattern (Fig. 4b). In general, the divergence patterns were consistent with those suggested, but not exactly observed, by Salas-Monreal and Valle-Levinson (2009) in the sense that convergence developed upstream of the pit and divergence appeared downstream. The divergence pattern emerged in both phases of the tidal cycle. In these observations, it is evident that the divergence

patterns were stronger and more robust in the flood phases than in the ebb phases of the tide. This asymmetry develops because the convergence pattern acts with the baroclinic pressure gradient to accelerate the flow toward the pit during flood but acts against the pressure gradient acceleration during ebb (Cheng and Valle-Levinson, 2009).

c. Baroclinic pressure gradient influence on tidal flow

The influence of the baroclinic pressure gradient on the flow speed V moving over a sinusoidal scour pit of length L and depth h_2, relative to the ambient depth outside the pit h_1, may be explained conceptually with a simplified, Bernoulli-type, frictionless momentum balance that yields (Cheng and Valle-Levinson, 2009):

$$V^2 = V_o^2 - 2g\eta - 2\frac{g}{\rho_o}\frac{\partial \rho}{\partial y}h_1 y - 2\frac{g}{\rho_m}\frac{\partial \rho}{\partial y}\frac{h_2 L}{\pi}\left[1 - \cos\left(\frac{\pi y}{L}\right)\right], \quad (1)$$

where V_o is the flow speed as it enters the pit, y is the along-pit direction, η is the sea surface elevation, g is the acceleration caused by gravity, ρ_o is a reference water density and $\partial\rho/\partial y$ is the along-pit horizontal density gradient. Note that the flow entering the pit V_o will be reduced if the other three terms are positive. In particular, note that if the density gradient is positive, i.e. density increasing in the direction of the flow, as in ebb periods, then V will be reduced in the pit. Conversely, if the density gradient is negative as in flood phases of the tidal cycle, then the flow speed will increase over the pit. This conceptual argument was supported by numerical solutions (Cheng and Valle-Levinson, 2009).

Returning to the observations in Kurushima Strait, the average ebb flows also depicted a deceleration over the scour pit as seen in the along-pit section (Fig. 5a). The cross-pit section also showed the largest along-pit current amplitude over the deepest part of the upstream section (Fig. 5c) but moving to the slopes on the downstream cross-section (Fig. 5b). The lateral flow patterns were rather vague on both cross-sections, unlike the average patterns observed during flood (Fig. 3b, c).

d. Vertical component of the flow

It is noteworthy, as an aside, that most fields recorded with the towed ADCP exhibited coherent patterns that followed the bathymetry. For instance, the vertical flow showed an overall descending pattern as the ebb flow entered the pit and an ascending pattern on leaving the pit (Fig. 6a). There were also coherent undulations of order 200 m wavelength likely triggered by the small mount (or megaripple) appearing at a distance of 3.7 km. The undulations were reasonably well resolved as the spatial precision of the averaged measurements was ~20 m. Although the overall descending/ascending flow pattern is expected for a fluid moving past a hole in the bottom, its observation with a towed ADCP, which tends to move up and down while at tow, was unanticipated. A similar vertical flow structure could be gleaned from the flood flow (Fig. 6b) in the deepest part of the scour pit, where the flow followed the bathymetry. Furthermore, the vertical component of the flow closely followed the megaripples that appeared on the edges of the channel. The

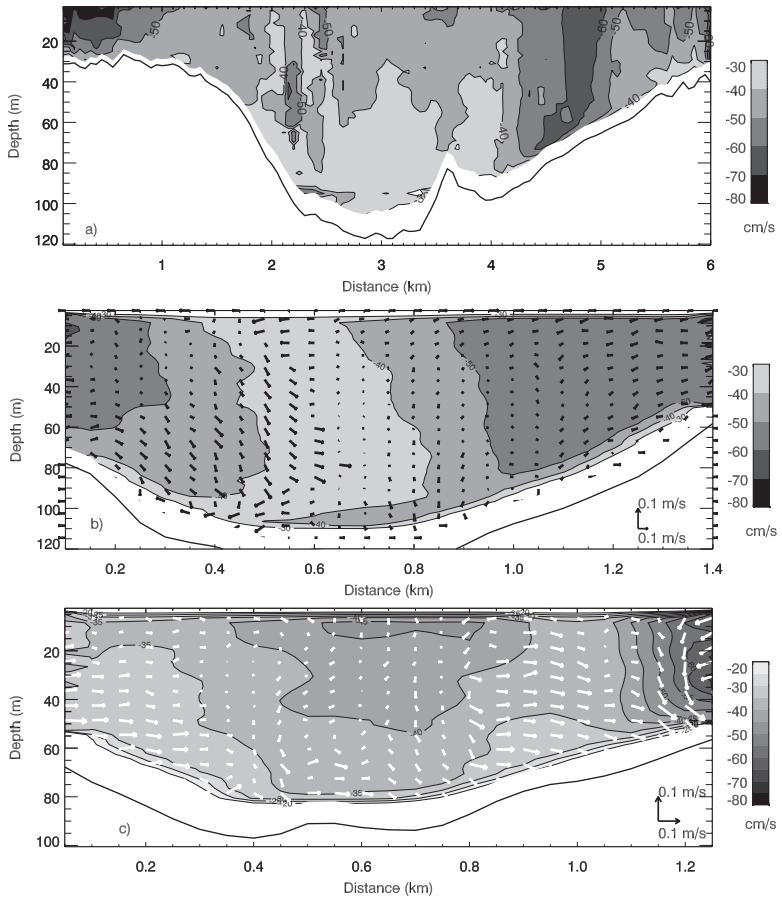

Figure 5. Temporal averages of the observations collected during ebb phases of the tidal cycle (same as Fig. 3, but for ebb). Flow moves from right to left on (a) and away from the observer on (b) and (c).

megaripples, like the flow undulations, are roughly 200 m in wavelength and 5–10 m tall, and therefore tend to modify the flow. The ripples actually seem to affect the entire water column, as seen in Figure 6. The interaction of the tidal flow with such ripples generates barotropic waves with wavelengths of the order of the bathymetry and heights that are one order of magnitude smaller than the ripple height. These wave properties are visual estimates derived from the surface expression of the waves.

e. Mean flow

The tidally averaged flow resulting from the interaction with the scour pit is shown in Figure 7. Both the tidally averaged surface flow and the tidally averaged depth-mean flow are included to show that the mean flow had practically no vertical structure. These flow

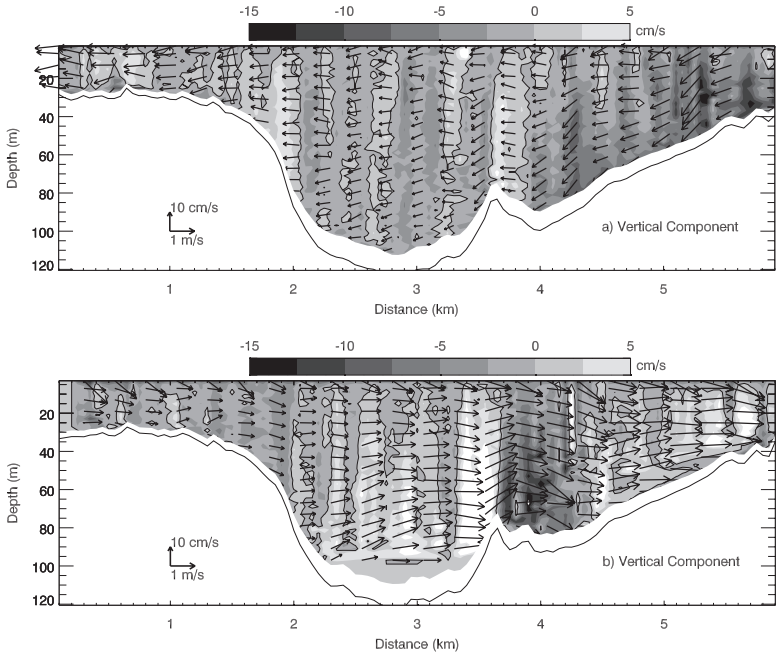

Figure 6. Contours of vertical component of velocity (in shades) for (a) ebb and (b) flood stages of the tidal cycle. Horizontal arrows represent the direction of flood or ebb.

fields were derived from the tidal average obtained along the sampling trajectory and then interpolated onto a uniform grid through Delaunay triangulations (e.g., Fang and Piegl, 1992, 1993). The mean fields depicted mainly northeastward flow with convergence on the southwestern flank of the pit and divergence on the northeastern flank. The convergence/divergence pattern seems to be part of a pair of recirculating gyres: a counterclockwise gyre over the northwestern part of the pit and flanks and a clockwise gyre over the southeastern part. Obviously, a geographically more extensive sampling trajectory is needed to resolve these gyres. Along the longitudinal axis of the pit, the net flow is in the flood direction, which likely results from the asymmetric enhancement of tidal flood flows over the pit. This agrees with the direction of the baroclinic pressure gradient force. The dynamical implications of such flow patterns are explored next in the Discussion section.

5. Discussion

This section concentrates on exploring the dynamical implications associated with the asymmetric flow patterns over the scour pit from flood to ebb tides. In particular, it is essential to determine the role of the horizontal density gradient, in terms of the baroclinic pressure gradient, in causing such asymmetry, as suggested by Cheng and Valle-Levinson (2009) and Eq. (1). Also, it is essential to determine whether frictional or inertial

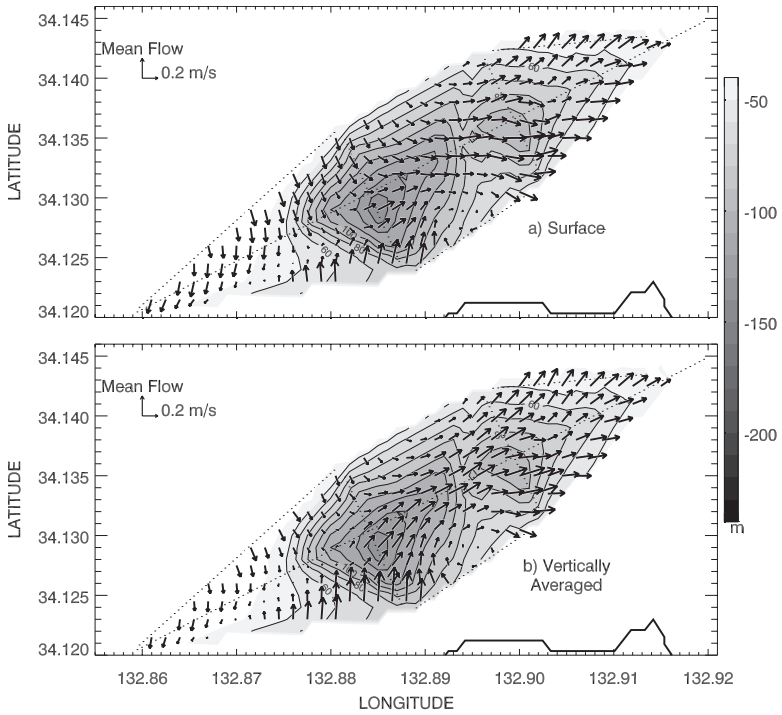

Figure 7. Residual flow after one tidal cycle (a) at the surface and (b) depth-averaged. The fields are very similar, which illustrates practically no vertical structure in the mean flows. Flows are drawn over the bathymetry (scale shown on right) of the scour pit.

(advective) effects are responsible for balancing the influence of the pressure gradient. It has been proposed that frictional effects balance the pressure gradient outside the pit and inertial effects become more dominant in the pit (Salas-Monreal and Valle-Levinson, 2009; Cheng and Valle-Levinson, 2009). These observations offer the opportunity to explore those concepts further. In order to investigate the ideas presented above and the dynamical implications, the spatial structure of four variables is described. The four variables are the vertically averaged flow, the volume transport per unit channel width, the advective or inertial accelerations in the momentum balance and the frictional terms. These four variables are calculated for flood periods and compared to those calculated for ebb periods.

During the flood phase of the tidal cycle, the vertically averaged along-pit flow, calculated from the temporal mean of all flood measurements (Fig. 3a), showed an increase over the pit (Fig. 8a, shaded region) but also as the tidal flow came out of the pit toward the shallow water column. However, the transport per unit width (m^2/s) was a mirror image of the bathymetry, increasing only over the pit (Fig. 8b, shaded region). This was an indication of mass convergence toward the pit during this phase of the tidal cycle, as

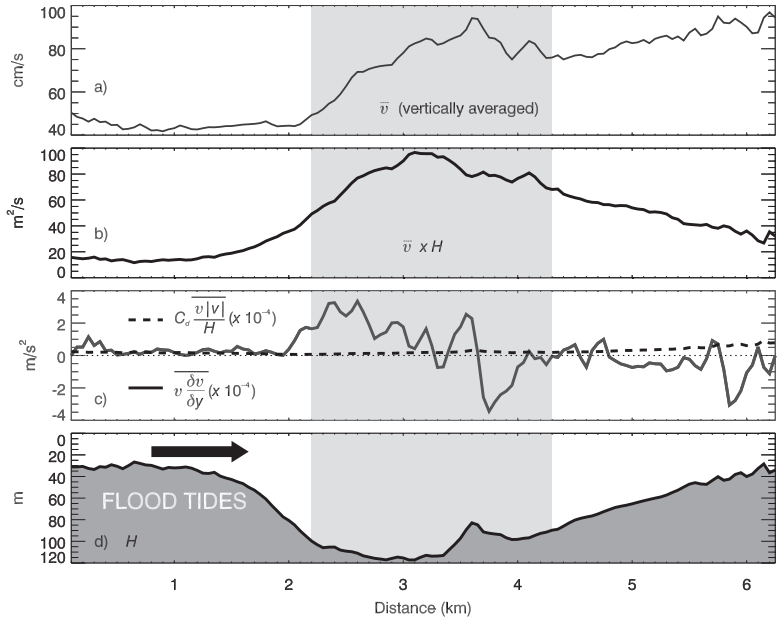

Figure 8. (a) Depth-averaged flow, (b) transport per unit width, (c) dynamical terms, and (d) bottom profile for flood phases of the tide. Overbars denote vertically averaged quantities.

illustrated in Figures 2b and 3b. The decrease in transport outside the pit, despite the acceleration of the tidal flow, was consistent with the mass divergence illustrated in Figures 2c and 3c.

With respect to the dynamic terms, frictional effects F (in m/s^2) were represented through parameterization of the bottom stress τ_b:

$$F = \frac{\tau_b}{\rho_o H} = \frac{\overline{C_b v[V]}}{H} \tag{2}$$

where ρ_o, as before, is a reference water's density, H is the water column depth, which varies with distance along the pit, C_b is a bottom drag coefficient taken as 0.003, v is the along-pit flow, V is the flow speed and the overbar indicates depth-averaged quantities. These frictional effects are compared to the advective effects, calculated with the along-pit flow as $\overline{v\partial v/dy}$, where ∂y is the spatial resolution of the measurements (20 m). Figure 8c shows that the inertial or advective term is larger than the frictional term over the deepest part of the pit (distance 2–4 km). Over the shallower parts (distance 4–6 km) of the pit the dominance becomes less evident and advection even becomes comparable to the frictional term in places, as it is before and on entering the pit (before the shaded area).

The competition between advection and bottom friction can be characterized by scaling these terms. Friction may be scaled as $C_b V_s^2/H$ and advection as V_s^2/L, where V_s is a

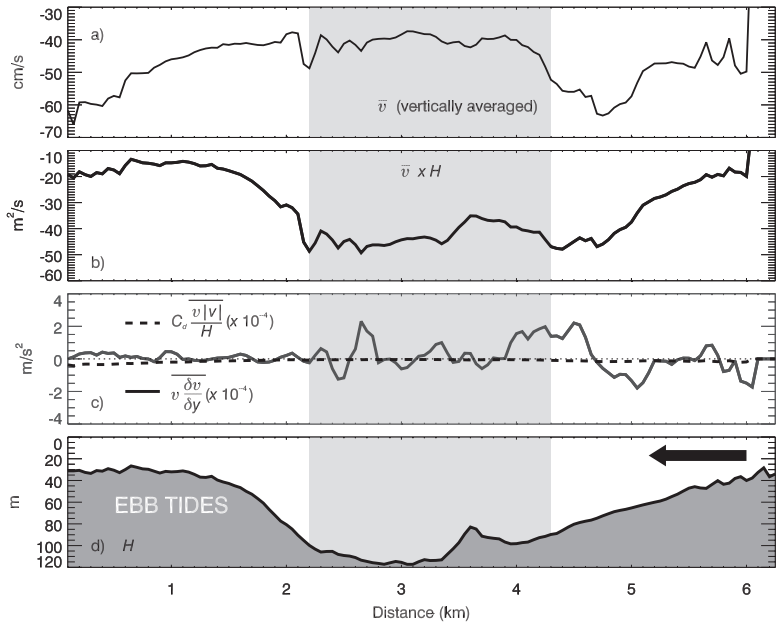

Figure 9. Same as Figure 8 but for the ebb phase.

velocity scale and L is a horizontal length scale. The velocity scale is really irrelevant because it vanishes upon comparing both dynamic terms. Such comparison yields that both terms are the same when C_b equals H/L or the bottom slope. From this scaling it can be said that inertia will dominate over friction where the bottom slope is greater than C_b $\sim$0.003. On the other hand, friction will dominate where H/L is smaller than C_b, (e.g., Salas-Monreal and Valle-Levinson, 2009). This can help explain why the advective term is greater than friction in the pit and suggests a change in the dynamics governing the motion over the pit relative to the shoals surrounding it. This difference is also observed during the ebb phase of the tidal cycle.

During ebb, the vertically averaged along-pit flow, calculated from the temporal average of the ebb flow observations (Fig. 5), shows a clear decrease in the pit (Fig. 9a, shaded region), after an initial increase (between $\sim$4 and 5 km). Such a decrease is expected from Bernoulli-type dynamics in which the flow speed decreases as it goes through an expansion of the cross-section (e.g., Eq. (1) with no density gradient). This was in contrast to the acceleration observed during flood (Fig. 8a) and also consistent with the effects of the baroclinic pressure gradient opposing the ebb tidal flows more strongly at greater depths. On the other hand, the transport per unit width shows an increase over the pit (Fig. 9b, shaded region). This increase is caused, as discussed in the description of the flow fields during ebb, by convergence of mass from the sides of the pit. In terms of the dynamical implications, the inertial or advective accelerations again become larger than frictional effects over the pit (Fig. 9c, shaded region). The transition where advection begins to

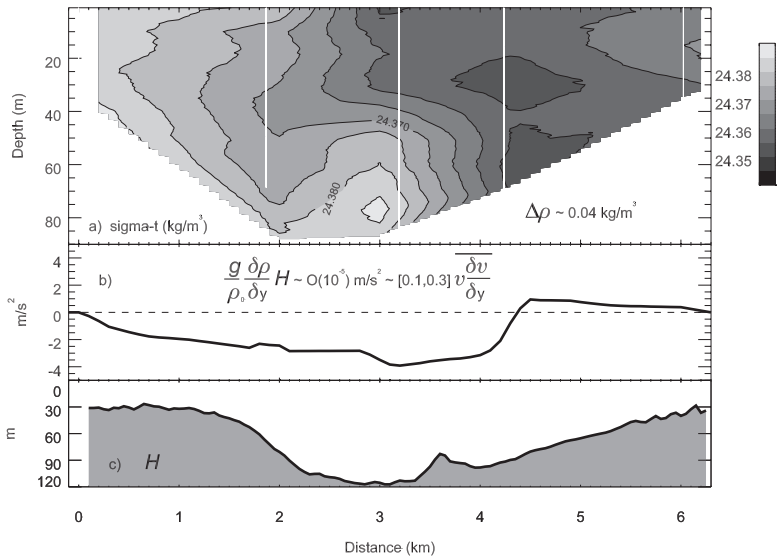

Figure 10. Distribution of (a) water density along the pit (white symbols represent location of measurements), (b) baroclinic pressure gradient along the bottom of the along-pit section, and (c) bathymetry of the along-pit section.

dominate over bottom friction in the dynamical balance emerges again where the bottom slope approximately equals the bottom drag (0.003).

It appears then that there is convergence of mass toward the pit at both flood and ebb phases and that the competition between advective and frictional accelerations is similar at both tidal phases. The question that arises then is what causes the convergence to be stronger during flood and an acceleration of the tidal flow during flood and deceleration during ebb? As suggested in the last sentence of the *Ebb phase* subsection of the Data Description section (section 4) and by the conceptual analysis of Eq. (1), the answer belies in the influence of the baroclinic pressure gradient on the tidal flow (Cheng and Valle-Levinson, 2009). Even though hydrographic profiles exhibit rather weak vertical stratification and weak horizontal density gradients (0.04 kg/m^3 in 6 km of the along-pit transect) (Fig. 10a), the baroclinic pressure gradient along the hollow is not negligible (Fig. 10b). The values calculated from the along-pit transect of Figure 10a are of order 10^{-5} m/s^2 or 10 to 30% of the advective accelerations. This is because the baroclinic pressure gradient is proportional to the depth of the water column, which exceeds 100 m in the pit. These observations support the model results of Cheng and Valle-Levinson (2009) that indicate that the essential ingredient for the flood/ebb asymmetries in the speed of the tidal flows over the pit is the presence of a baroclinic pressure gradient influence. It is this gradient that causes asymmetric convergence patterns from flood to ebb. During flood, the baroclinic pressure gradient acts in conjunction with the barotropic pressure gradient that drives the tidal flow. The superposition of forces increases with depth and causes the

near-bottom acceleration in the pit during flood. During ebb, the tidal flood is hindered at depth by the baroclinic pressure gradient, most effectively in the great depths of the pit.

It can be reasonably argued that the flow patterns observed in this part of the Seto Inland Sea may also be produced by the headland, Kajitori-no-ha, protruding toward the scour pit (Fig. 1). The headland is expected to favor convergence of mass toward the hollow during flood phases of the tide and divergence during ebb phases of the tide. The convergence of mass produced by Kajitori-no-ha is likely to produce flood flow accelerations over the pit. However, the observed accelerations are better distinguished near the bottom, instead of at the surface or throughout the water column as should be expected from the effects of the headland. Moreover, the numerical results that indicated flow accelerations over a scour pit during flood phases of the tide, the same results that motivated this study (Cheng and Valle-Levinson, 2009), were obtained for a channel of constant width. The numerical model results indicated that the horizontal density gradient causes the asymmetries observed in this study. Those two details (a) the fact that the observed flood flow accelerations are most prominent near the bottom than at the surface, and (b) the agreement of the numerical results obtained in a straight channel with our observations, strongly suggest that the change in channel width plays a secondary role in the flood flow accelerations over the scour pit. Further numerical simulations that examine the presence of a headland near the scour pit will better elucidate the relative role played by morphology and by density gradients on the flow patterns observed.

6. Conclusion

The main finding of this study was that asymmetries in the tidal flow from flood tide to ebb tide over a scour pit can develop even under seemingly homogeneous hydrography. However, careful attention must be paid to the size of the baroclinic pressure gradient because ultimately it is the main agent that causes the asymmetry. This study also confirms previous assertions of the transition in dynamics from friction-influenced flow outside the pit to advection-dominated flow inside the pit. The transition may be found where the bottom slope at the pit equals the bottom drag coefficient ($\sim$0.003).

Acknowledgments. The authors express their sincere gratitude to Mr. H. Ohnishi, the captain of R. V. *Tobiuo* and to Drs. P.-H. Chang and D. Takahashi for their valuable help with the field work. X. Guo was supported by a Grant-in-Aid for the Global COE Program from the Ministry of Education, Culture, Sports, Science and Technology, Japan (MEXT), and the Japan Society for the Promotion of Science (JSPS). AVL acknowledges support from the U.S. National Science Foundation projects 0551923 and 0726697. The manuscript was completed while AVL was on leave at the Centre for Water Research, University of Western Australia (2294).

REFERENCES

Armi, L. 1986. The hydraulics of two flowing layers with different densities. J. Fluid Mech., *163,* 27–58.

Cheng, P. and A. Valle-Levinson. 2009. Spatial variations of flow structure over estuarine hollows. Cont. Shelf Res., *29,* 927–937.

Davies, A. G. and J. M. Brown. 2007. Field measurement and modelling of scour pit dynamics in a sandy estuary. *Coastal Sediments'07,* 1–14.

Fang, T. and L. Piegl. 1993. Delaunay triangulation using a uniform grid. IEEE Computer Graphics and Applications, *13,* 36–47.

—— 1992. Algorithm for Delaunay triangulation and convex hull computation using a sparse matrix. Computer Aided Design, *24,* 425–436.

Farmer, D. M. and L. Armi. 1986. Maximal two-layer exchange over a sill and through the combination of a sill and a contraction with barotropic flow. J. Fluid Mech., *164,* 53–76.

Park, M-L. and D. P. Wang. 1991. Transient tidal vorticity over a hollow, *in* Tidal Hydrodynamics, B. B. Parker, ed., Wiley, NY, 419–434.

Salas-Monreal, D. and A. Valle-Levinson. 2009. Continuously stratified flow dynamics over a hollow. J. Geophys. Res., *114,* C03021, doi:10.1029/2007JC004648.

Stenström, P. 2003. Mixing and recirculation in two-layer exchange flows. J. Geophys. Res., *108(C8),* 3256, doi:10.1029/2002JC001696.

Yanagi, T. and T. Okaichi. 2007. Seto Inland Sea—Historical Background, Chapter 2, *in* Sustainable Development in the Seto Inland Sea, Japan—From the Viewpoint of Fisheries, T. Okaichi and T. Yanagi, eds., Terra Sci. Pub., Tokyo, Japan, 9–14.

Yanagi, T., H. Takeoka, and H. Tsukamoto. 1982. Tidal energy balance in the Seto Inland Sea. J. Oceanogr. Soc. Jap., *38,* 293–299.

Received: *11 June, 2009;* revised: *27 October, 2009.*